

## Particle Interactions with Matter

A. Lechner

CERN, Geneva, Switzerland

### Abstract

With steady advances in accelerator technology and new records in beam energy, intensity, brightness, power, and luminosity, it is essential to limit the adverse effects of beam losses for accelerator operation, equipment, and personnel. Particle losses can quench superconducting magnets, induce single-event effects in electronics, activate equipment, and alter material properties. In the worst case, high-energy particle beams can cause severe damage to equipment, if they are lost in an uncontrolled way. Modern accelerators typically rely on a system of protection absorbers, dumps, and beam manipulation devices to safely accelerate, store, extract, and transfer beams. Knowledge of particle–matter interactions is important to understand and predict the consequences of beam losses and to design beam-intercepting devices, shielding, and other equipment. This paper summarizes the principal physical processes of hadrons, photons, and leptons in matter and discusses related phenomena, such as particle showers.

### Keywords

Particle–matter interactions; particle showers; energy deposition.

## 1 Introduction

All particles of a beam or their secondary interaction or decay products will eventually interact with surrounding matter. Depending on the particle type and energy, swift particles penetrating in a material will be subject to different atomic and nuclear processes. The complexity of particle–matter interactions can be illustrated for the example of high-energy protons: if high-energy protons ( $\geq$ GeV) impact on a material, they are subject to inelastic nuclear collisions, producing, on average, a number of fast secondary hadrons; some of these hadrons (protons, neutrons, charged pions) can have further nuclear collisions, resulting in a hadronic cascade; others (neutral pions) will decay almost instantly and their decay products ( $\gamma$ -pairs) can initiate electromagnetic showers, which are sustained by electron–positron pair production by photons and Bremsstrahlung losses of electrons and positrons. As the particle energy decreases, other processes become dominant (Compton scattering of photons, photoelectric effect, ionization losses of charged particles). Some of the charged pions and other hadrons will also decay and produce muons. Besides the production of fast hadrons, nuclear collisions also give rise to lower-energy (MeV) neutrons, protons, light ions (alpha particles) and gamma rays, which are emitted during the de-excitation of target nuclei. The protons and light ions will mainly range out because of ionizing losses. The neutrons can, however, be very penetrating and will mainly undergo elastic nuclear collisions until they thermalize and are captured. Eventually, the residual nuclei of elastic and inelastic collisions can also recoil and impart their energy on neighbouring nuclei through Coulomb interactions. This description provides only a glimpse of the copious particle production mechanisms in high-energy particle interactions in matter.

The interactions of particles in accelerator equipment can have many different negative consequences, from instantaneous damage or long-term damage of equipment because of shock heating or atomic displacements to the activation of equipment because of radionuclei production in nuclear collisions. Knowledge of particle–matter interactions is therefore essential for designing and operating new accelerators in order to mitigate consequences for equipment and personnel. This paper provides a very basic introduction to beam–matter interactions for a non-expert audience working in the field of

particle accelerators who seeks to get a first understanding of the topic. The paper aims to convey a basic overview of the relevant physical processes and related phenomena, such as particle showers, without an in-depth discussion of the underlying theories. It introduces commonly used definitions and quantities and describes the dependencies of processes and energy deposition profiles on particle energy and target material. The paper is partially based on previous papers by Ferrari [1, 2]. Particle–matter interactions in accelerators have also been discussed in another paper by Mokhov and Cerutti [3]. The reader is referred to these papers for additional and complementary information. In addition, a wealth of literature is available, where the physical processes and in particular the underlying theories and models are discussed in much greater detail (see, for example, Refs. [4–7]). The paper is organized as follows. Section 2 gives a brief introduction of beam-intercepting devices, sources of secondary particles, and consequences of particle–matter interactions. Section 3 summarizes the properties of relevant particles and discusses the relation between cross-section, mean free path, and interaction probability. Sections 4 and 5 provide a basic account of atomic and nuclear processes and Section 6 concludes the paper, with a discussion of energy deposition profiles and particle showers.

## 2 Beam–machine interaction

### 2.1 Particle impact on beam-intercepting devices

Particle accelerators employ a variety of beam-intercepting devices, such as collimators, scrapers, dumps, stripping foils, crystals, or targets. These devices serve different purposes, such as machine protection, reduction of activation in certain areas, beam extraction, or particle production for experiments. A few examples are listed in the following.

- *Beam disposal on dumps.* In case of a beam abort, which can be deliberate or due to an emergency situation, the beam is steered onto a beam dump or a beam stopper, which should absorb a large fraction of the energy carried by the beam particles. Beam dumps must be robust enough to sustain the impact of full bunch trains stored in a machine or transferred between machines. Design features of a dump, such as the choice of absorber materials, dimensions, cooling circuits, etc., depend on the particle type and energy, as well as on operational parameters, such as the beam intensity, the beam brightness, and the dumping frequency. In high-energy hadron colliders, such as the LHC, beam dumps can be as long as 10 m and need to be surrounded by heavy shielding to reduce the activation of the environment [8]. In addition, the LHC beams need to be swept transversally across the dump front face by dilution kickers to avoid excessive temperatures and stresses in the graphitic dump core [8].
- *Machine protection and beam manipulation.* Beam particles can be intercepted by protection or beam manipulation devices, such as collimators, absorbers, or scrapers, which are usually placed in close proximity to the beam. Such devices are employed for different reasons, for example, to remove unwanted halo particles before they are lost in sensitive locations, such as superconducting magnets; to protect the machine in case of equipment malfunction (e.g., mis-steering of the beam during injection or asynchronous beam dumps); to reduce the background to experiments; or to concentrate losses in a certain location for radioprotection reasons. The latter can be crucial to limit the exposure of personnel during technical interventions.
- *Beam extraction.* The physical interaction of beam particles with different devices is exploited in certain extraction techniques. Beam particles can, for example, be extracted by changing their charge using a stripping foil. In other cases, bent crystals are used to selectively steer beam particles. Charged particles impacting on a crystal can be subject to different coherent phenomena, such as channelling or volume reflection, which have been successfully exploited for beam manipulation and extraction. Particles that do not have the right impact angle with respect to the crystal planes or that are de-channelled, interact with the crystal, as they would with an amorphous absorber.

- *Particle production in targets.* In many cases, beam particles are directed onto a fixed target to produce secondary particles for physics experiments or diagnostic purposes. The target design requirements depend on the specific use case, in particular on the type and spectrum of secondary particles to be produced. A typical example is the production of neutrons in spallation targets. Spallation targets can be solid (e.g., lead) or liquid (e.g., mercury) and are usually combined with a moderator (e.g., heavy water) to manipulate the neutron spectrum.

## 2.2 Sources of secondary particles

Not only beam particles but also secondary particles might interact with surrounding equipment. The production of secondary particles can be localized or spread across a machine. A few examples are given here.

- *Luminosity production.* Secondary particles are produced in the interaction points of a collider, where two beams are brought into collision. A fraction of the collision products may escape the experimental cavern and can interact with nearby accelerator equipment [9, 10].
- *Beam–gas collisions.* Other sources of secondary particles are interactions of beam particles with residual gas molecules in the vacuum chamber. Hadron beams can have inelastic nuclear encounters with gas nuclei, resulting in the production of secondary hadrons, muons, or photons, which can, for example, be a source of background to experiments [11]. Electron or positron beams can be subject to Bremsstrahlung losses.
- *Dust or macroparticle-induced losses.* Beam losses can also be induced by dust particles liberated into the beams. First observed in electron storage rings, where ionized dust particles were found to be trapped in the beam [12], they have also been observed in the LHC [13, 14], where they triggered many beam aborts and even magnet quenches. In electron machines, dust trapping can lead to Bremsstrahlung losses in the field of a charged macroparticle; this is generally referred to as duststrahlung [12].
- *Synchrotron radiation.* Synchrotron radiation is emitted if charged particles are bent by a magnet or if they are accelerated. Synchrotron radiation can be a significant source of beam power loss in circular electron and positron machines.

## 2.3 Consequences of particle–matter interactions for operation, equipment, and personnel

Particle interactions with matter can have negative consequences for an accelerator, leading to disruptions of machine operation or causing long-term effects. A few particle-induced effects are summarized in the following.

- *Activation of equipment.* Nuclear interactions lead to the activation of accelerator equipment [15]. Radioisotopes are not only produced in hadron machines, but also in electron accelerators because of photonuclear and electronuclear interactions. The types of radionuclides produced in a material depend on the elemental composition and decay chains. Activation of equipment may require access restrictions or dedicated cooling times before technical intervention. Radioactive isotopes can also be produced in the surrounding environment (soil, air, ground water), which may require special monitoring.
- *Long-term radiation damage of equipment.* Long-time exposure to radiation can lead to the embrittlement and swelling of materials and may degrade physical material properties, such as electrical or thermal conductivity. Radiation damage in non-organic materials is generally related to gas production (H, He) in nuclear reactions and to the displacement of atoms from the lattice due to the non-ionizing energy loss of particles. Atomic displacements depend on the damage threshold of a material. Organic materials can change their properties if they receive a large ionizing dose.

Organic insulators are, for example, used in some magnet coils and adequate shielding might be necessary in high-radiation areas to avoid degradation of the material properties.

- *Instantaneous damage of equipment because of thermal shock.* In the case of an uncontrolled fast beam loss on the aperture, the stresses generated by beam-induced thermal shock can lead to instantaneous material damage. Damage can occur when the energy densities reach the order of  $\text{kJ/cm}^3$  (depending on the material properties and the spatial energy density distribution). If the beam-induced energy density is high enough, materials can even be subject to a phase transition (melting). Equipment damage can be very disruptive for operation and may lead to weeks of downtime for repairs. Particle beams in a high-energy collider, like the LHC, with a stored energy of hundreds of MJ, have an enormous damage potential. The LHC employs a sophisticated machine protection system, which extracts the beams on the dump block if equipment is found to be malfunctioning or if beam losses measured by beam loss monitors exceed a certain threshold [8]. The LHC employs, in addition, a multistage collimation system with robust collimators made of carbon-reinforced carbon, which provide another layer of protection [8].
- *Quenches of superconducting magnets.* If the beam-induced energy deposition in the coils of a superconducting magnet exceeds a certain level, the magnet can quench, i.e., it can become normally conducting. The minimum energy density to induce a quench depends on the beam loss duration, the coil geometry, the superconductor type, the magnet current, and the operation temperature. Quench levels are orders of magnitude less ( $\sim \text{mJ/cm}^3$ ) than the damage limit of coils. A magnet quench can lead to a machine downtime of several hours. In high-energy machines, such as the LHC, a small fraction of beam particles ( $\sim 10^{-7}$ ) can induce a quench if lost on the magnet aperture [16]. The risk of beam-induced magnet quenches must be assessed in the design phase of a superconducting machine and appropriate measures must be implemented (e.g., collimators, shielding inserts in magnets, beam loss monitors).
- *Radiation effects in electronics.* Electronics exposed to radiation fields can suffer single-event effects, which can be non-destructive or destructive. Even if non-destructive, single-event effects can limit the performance of an accelerator by triggering beam aborts [17]. Over longer periods, electronics can also be compromised by cumulative displacement damage or the total ionizing dose deposited by charged particles.

### 3 Particles and interaction probability

#### 3.1 Particle types and properties

If a beam particle interacts with matter, secondary particles can be produced in atomic and nuclear processes, as illustrated in the example given in Section 1. Table 1 summarizes the mass, mean life  $\tau$ , and main decay mode of the most relevant particle species found in hadron and lepton accelerator environments. Photons are present in high abundance in most machines. They are produced in Bremsstrahlung processes of charged particles, in electron–positron annihilation, in gamma de-excitation after nuclear reactions, in radiative neutron capture, or in the decay of particles (e.g.,  $\pi^0$  decay). The most common hadrons are protons, neutrons, pions, and also other species, such as kaons (the latter are not included in the table). Hadrons can be produced in inelastic hadron–nucleus collisions, but also in other processes, such as photonuclear reactions. Neutrons can be very penetrating, since they are neutral and have a relatively long mean lifetime of almost 15 min. Pions are the lightest hadrons and hence are produced with high multiplicities in nuclear collisions. Although charged pions are unstable, their mean range is sufficiently long that they typically reinteract in a material before decaying. Neutral pions have a much shorter lifetime and range and they decay predominantly into a  $\gamma$ -pair. They are the main source of electromagnetic showers in high-energy hadron machines. The most copiously produced leptons are electrons, positrons, and muons. Electrons are released in Coulomb interactions of charged particles and in various photon processes (photoelectric effect, Compton scattering, and electron–positron pair

**Table 1:** Particle properties (from Ref. [4])

	Particle type	Rest mass [MeV/c]	Mean life $\tau$ [s]	Main decay mode
Photons	( $\gamma$ )	0	Stable	–
Leptons	Electron ( $e^-$ ), positron ( $e^+$ )	0.511	Stable	–
	Muon ( $\mu^+$ , $\mu^-$ )	105.66	$2.2 \times 10^{-6}$	$\mu^- \rightarrow e^- \bar{\nu}_e \nu_\mu$ $\mu^+ \rightarrow e^+ \nu_e \bar{\nu}_\mu$
Hadrons	Proton (p)	938.27	Stable	–
	Neutron (n)	939.57	880	$n \rightarrow p e^- \bar{\nu}_e$
	Charged pion ( $\pi^+$ , $\pi^-$ )	139.57	$2.6 \times 10^{-8}$	$\pi^- \rightarrow \mu^- \bar{\nu}_\mu$ $\pi^+ \rightarrow \mu^+ \nu_\mu$
		Neutral pion ( $\pi^0$ )	134.98	$8.5 \times 10^{-17}$

production). Muons are mainly produced in the decay of pions and kaons.

### 3.2 Cross-section and mean free path

The collision probability of an incident particle with an atom (or nucleus) with atomic number  $Z$  and mass number  $A$  is generally quantified by the microscopic cross-section,

$$\sigma = \sigma(E, Z, A). \quad (1)$$

The microscopic cross-section depends on the projectile type and the projectile energy  $E$  and is often interpreted as the effective area for a collision. Cross-sections are generally expressed in terms of barns ( $1 \text{ b} = 10^{-24} \text{ cm}^2$ ). Considering a particle travelling inside a material, the average distance between two successive collisions, i.e., the mean free path  $\lambda$ , is then given by

$$\lambda = \frac{1}{N\sigma} = \frac{M}{\rho N_A \sigma}, \quad (2)$$

where  $N$  is the atom density,  $M$  is the molar mass,  $\rho$  is the material density, and  $N_A$  is the Avogadro constant ( $6.022045 \times 10^{23} \text{ mol}^{-1}$ ). In the case of a material mixture, the mean free path becomes

$$\lambda = \frac{1}{\sum_i N_i \sigma_i} = \frac{1}{\rho N_A \sum_i (\omega_i / M_i) \sigma_i}, \quad (3)$$

where  $\sum_i$  is the sum over all elemental constituents,  $N_i$  is the atom density of element  $i$ ,  $M_i$  is the molar mass of element  $i$ , and  $\omega_i$  is the relative weight fraction of element  $i$  in the mixture. The inverse of the mean free path is generally referred to as the macroscopic cross-section  $\Sigma$ ,

$$\Sigma = \frac{1}{\lambda}. \quad (4)$$

In contrast with the microscopic cross-section in Eq. (1), the unit of the macroscopic cross-section is the unit of an inverse length, usually expressed in  $\text{cm}^{-1}$ . When quantifying particle penetration in matter, the amount of material traversed is often expressed as the product of length (cm) and material density ( $\text{g/cm}^3$ ), which is also referred to as the surface density ( $\text{g/cm}^2$ ). Surface density units are often used for the mean free path and macroscopic cross-section:

$$\lambda' = \lambda\rho, \quad \Sigma' = \frac{1}{\lambda\rho}. \quad (5)$$

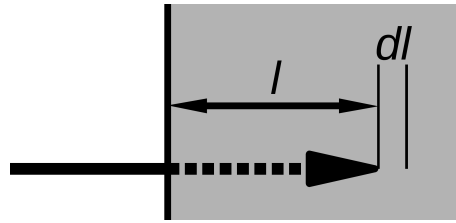


Fig. 1: Path length  $l$  of a particle inside a target.

### 3.3 Interaction probability

Assume that particles are normally incident on a homogeneous material and that they are subject to a process with a mean free path  $\lambda$  between collisions. Let us denote by  $l$  the distance travelled by a particle inside the material, as illustrated in Fig. 1. Then the probability that a particle suffers a collision between  $l$  and  $l + dl$  is given by

$$p(l)dl = \frac{1}{\lambda} \exp\left(-\frac{l}{\lambda}\right)dl. \quad (6)$$

By definition, the integral of  $p(l)dl$  over a semi-infinite target yields unity,

$$\int_0^{\infty} p(l')dl' = 1, \quad (7)$$

and the first moment of the probability density function  $p(l)$  is  $\lambda$ ,

$$\int_0^{\infty} p(l')l'dl' = \lambda. \quad (8)$$

The probability that a particle has an interaction up to a path length  $l$  is then given by the cumulative distribution function

$$P(l) = \int_0^l p(l')dl' = 1 - \exp\left(-\frac{l}{\lambda}\right). \quad (9)$$

It follows from this expression that 63.2% of all particles will have a collision up to a path length of  $\lambda$ , 86.5% will have a collision within  $2\lambda$ , 95% within  $3\lambda$ , and 98.2% within  $4\lambda$ . For a thin target, i.e., for a target thickness  $d \ll \lambda$ , the exponential term in Eq. (9) can be expanded into a Taylor series and  $P(l)$  can be approximated as

$$P(d) \Big|_{d \ll \lambda} = 1 - \exp\left(-\frac{d}{\lambda}\right) = 1 - \left(1 - \frac{d}{\lambda} + \dots\right) \approx \frac{d}{\lambda}, \quad (10)$$

i.e., the probability that the particle interacts in the target is simply given by the ratio of target thickness and mean free path. Analogous to the interaction probability, one can define the survival probability  $P_s(l)$ , i.e., the probability that a particle does not suffer a collision until a distance  $l$ ,

$$P_s(l) = 1 - P(l) = \exp\left(-\frac{l}{\lambda}\right). \quad (11)$$

It follows from this expression that the chance that a particle did not have an interaction up to a distance  $l$  falls off exponentially.

As a practical example of the particle survival in an absorber, let us consider the accidental loss of a 450 GeV proton bunch train during transfer from the CERN SPS to the LHC. A nominal LHC injection train comprises 288 bunches with a bunch intensity of  $1.15 \times 10^{11}$  protons, which gives a total intensity of  $I = 3.31 \times 10^{13}$  protons [8]. In the event of an extraction kicker erratic, a train can be

mis-steered and is then intercepted by collimators in the transfer line, which protect the transfer line and the LHC magnets from damage. Each of the SPS-to-LHC transfer line collimators is 1.2 m long and consists of graphite with a density of  $1.84 \text{ g/cm}^3$ . Let us assume that an entire LHC injection train impacts on a single collimator: how many beam protons would then survive the impact, i.e., how many beam protons would escape from the downstream face of the collimator? A beam proton ceases to exist if it is subject to an inelastic nuclear collision inside the collimator. Elastic scattering processes (nuclear elastic or Coulomb scattering) and energy loss processes (ionization) do not affect proton survival and are therefore not considered here. The inelastic nuclear cross-section  $\sigma_i$  for a 450 GeV proton colliding with a carbon nucleus is about 245 mb, as predicted by the FLUKA code [18, 19]. Using the molar mass of carbon (12.0107 g/mol) and the specified graphite density, one can calculate the mean free path of protons in the collimator (in this case also referred to as the inelastic scattering length):

$$\lambda = \frac{M}{\rho N_A \sigma_i} \quad (12)$$

$$= \frac{12.0107 \text{ g/mol}}{1.84 \text{ g/cm}^3 \cdot 6.022 \times 10^{23} \text{ mol}^{-1} \cdot 245 \times 10^{-27} \text{ cm}^2} \quad (13)$$

$$= 44 \text{ cm} . \quad (14)$$

Using Eq. (11), one can then derive the number of surviving beam protons:

$$I_s = I \cdot \exp\left(-\frac{l}{\lambda}\right) \quad (15)$$

$$= 3.31 \times 10^{13} \cdot \exp\left(-\frac{120 \text{ cm}}{44 \text{ cm}}\right) \quad (16)$$

$$= 2.2 \times 10^{12} . \quad (17)$$

This shows that 93.5% of the beam protons have an inelastic interaction in the collimator or, in other words, that the surviving proton intensity is equivalent to the intensity of 19 nominal bunches. It is to be noted that a large fraction of the initial energy of protons interacting in the collimator still escapes the absorber material in the form of particle showers. But contrary to the surviving beam protons, shower particles have different magnetic rigidities and they dissipate their energy in a more diluted way than focused proton bunches.

## 4 Atomic interactions

### 4.1 Photon interactions

Knowledge of photon interactions and absorption is important for most accelerator applications since photons are produced in a variety of processes. Several processes contribute to the scattering and to the absorption of photons in matter. Figure 2 illustrates the cross-sections of the different processes as a function of energy for carbon and lead. The different photon processes are as follows.

- *Coherent scattering or Rayleigh scattering.* The photon is subject to scattering from bound electrons without ionizing or exciting the atom. The recoil energy of the atom is generally negligible, i.e., the photon essentially retains its energy. The cross-section scales approximately with  $Z^2$ . Rayleigh scattering is only of marginal importance for many accelerator-related problems since it does not contribute to the absorption of photons.
- *Photoelectric effect.* The photon is absorbed and an electron is released from its atomic binding state. The photoelectric effect can only occur if the photon energy exceeds the binding energy  $U_i$  of an atomic shell. The energy of the emitted electron corresponds to the photon energy minus  $U_i$ . If the photoelectric effect involves an inner shell, the emission of an electron is typically followed by atomic relaxation. This means that the vacancy is filled by an electron from an outer shell

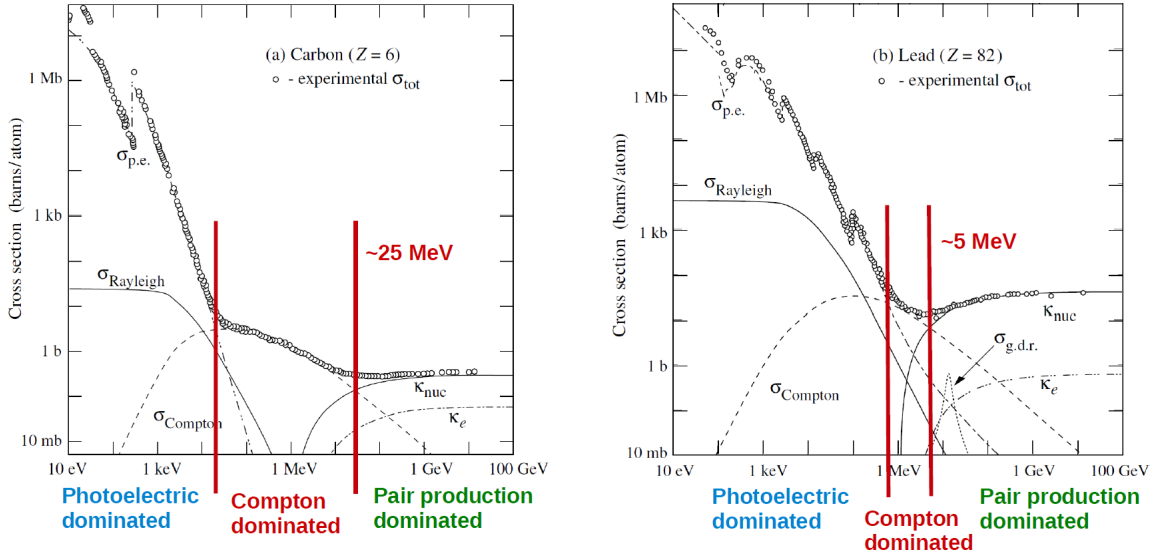


**Fig. 2:** Total cross-sections (circles) and partial cross-sections (lines) of photons in (left) carbon and (right) lead. The partial cross-sections correspond to the following processes: photoelectric effect ( $\sigma_{\text{p.e.}}$ ), coherent scattering ( $\sigma_{\text{Rayleigh}}$ ), Compton scattering ( $\sigma_{\text{Compton}}$ ), pair production in the field of the nucleus ( $\kappa_{\text{nuc}}$ ), pair production in the field of the electrons ( $\kappa_e$ ), and the giant dipole resonance ( $\sigma_{\text{g.d.r.}}$ ), which is a photonuclear process. The figure originates from Ref. [4].

and characteristic X-rays or Auger electrons are emitted. The photoelectric effect is the dominant photon process at lower energies (see Fig. 2). The cross-section scales approximately with  $Z^{4-5}$  and exhibits distinct absorption edges which reflect the prevalence for certain atomic shells once the photon energy exceeds the corresponding binding energy.

- *Incoherent scattering or Compton scattering.* A photon collides with an electron, imparts some of its energy to the electron and is scattered into a different direction. The energy imparted on the electron can amount from zero to a large fraction of the incident gamma energy. Compton scattering can also be followed by atomic relaxation. The Compton effect is the dominant photon process at MeV energies (see Fig. 2). The cross-section scales approximately with  $Z$ , i.e., it has a weaker dependency on the atomic number than the photoelectric effect and electron–positron pair production. The Compton-dominated energy range is therefore smaller for higher- $Z$  materials.
- *Electron–positron pair production.* At higher photon energies, pair production in the field of nuclei is the dominating absorption mechanism of photons. The threshold energy for electron–positron pair production is 1.022 MeV, i.e., the combined rest energy of an electron and a positron. The cross-section scales approximately with  $Z^2$ . The energy above which pair production dominates is less for higher- $Z$  materials (around 25 MeV for carbon and around 5 MeV for lead). Pair production is the relevant photon process in electromagnetic cascades. Since high-energy electrons and positrons can lose energy in Bremsstrahlung processes, new photons can be produced. Electromagnetic cascades are described in more detail in Section 6.

In addition to atomic processes, photons can also be subject to photonuclear interactions, which are not discussed here. In photon-related problems, the mean free path  $\lambda$  multiplied by the material density  $\rho$  is generally referred to as the mass attenuation length or absorption length, and the inverse is generally referred to as the mass attenuation coefficient,

$$\mu_m = \frac{1}{\lambda\rho} = \frac{N_A \sum_j \sigma_j}{M\rho}, \quad (18)$$

where  $\sum_j \sigma_j$  is the sum of cross-sections of all the processes discussed. The definition of the mass attenuation coefficient is identical to the macroscopic cross-section in surface density units (see Eq. (5)).

## 4.2 General remarks about charged particle interactions

Charged particles travelling inside a material are subject to Coulomb interactions with electrons and nuclei. As a consequence, the particles slow down and are deflected with respect to their initial direction.

- *Coulomb interactions with electrons lead to the excitation or ionization of atoms.* Energetic secondary electrons ejected in ionization processes are generally referred to as  $\delta$ -rays. Collisions with electrons dominate the energy loss of charged particles up to energies above which radiative loss becomes important, i.e., typically up to tens of MeV for electrons and positrons, up to a few hundred GeV for muons, and up to even higher energies for charged hadrons. High-energy hadrons are also subject to inelastic nuclear collisions, which play a major role in the energy dissipation in a material if the hadron energy is of the order of GeV or higher. However, nuclear collisions are less frequent than Coulomb interactions and high-energy hadrons still lose some energy in Coulomb interactions before being subject to a nuclear collision.

The energy loss due to Coulomb interactions with electrons is generally called electronic energy loss and leads to the heating of a material. In most Coulomb collisions, the energy transfer  $T$  is small (of the order of tens of eV), but cross-sections are large; hence, a charged particle will be subject to many collisions. In particle transport problems, the energy loss of charged particles is generally treated in a statistical way. Assuming that  $d\sigma(T)/dT$  is the differential cross-section for an energy transfer  $T$  to an electron, then the mean energy loss per unit path length, which is generally referred to as the electronic stopping power, is given by

$$\left. \frac{dE}{dx} \right|_{\text{elec}} = N \int_0^{T_{\text{max}}} T \frac{d\sigma}{dT}(T) dT, \quad (19)$$

where  $T_{\text{max}}$  is the maximum energy transfer, which can be derived from particle kinematics. Stopping powers of hadrons, muons, and electrons are shown in the following subsections. Energy loss fluctuations are equally important when studying the ionizing energy loss of charged particles (often described by the Landau–Vavilov distribution [20–22]), but are not further discussed in this paper.

- *Coulomb interactions with nuclei dominate the angular deflection of charged particles in a material.* Particles are subject to smaller deflections if their energy is greater. Lighter particles scatter more if they have the same  $\beta c$  as heavier particles. Like the energy loss in electronic collisions, deflections in collisions with nuclei are often treated in theories where the net effect of multiple events is studied (multiple scattering theories). Multiple Coulomb scattering is described well by the theory of Molière [23] (see also Ref. [24]).

The energy loss in collisions with nuclei is generally much smaller than the electronic energy loss, except for low-energy heavy projectiles (typically ions in the keV/u energy range). The energy loss is called non-ionizing energy loss and can lead to the displacement of atoms from the lattice if the energy transfer is higher than a certain material-dependent damage threshold, which can also depend on the particle direction in crystalline materials. In analogy to the electronic stopping power, the mean energy loss per unit length due to Coulomb collisions with nuclei is called the nuclear stopping power.

At higher energies, charged particles are also subject to radiative losses. Electrons with energies above a few tens of MeV are increasingly subject to Bremsstrahlung processes in the Coulomb field of nuclei, i.e., the electrons lose some of their energy, which is emitted in the form of a Bremsstrahlung photon. For other charged particles, radiative losses are only important at much higher energies because of their

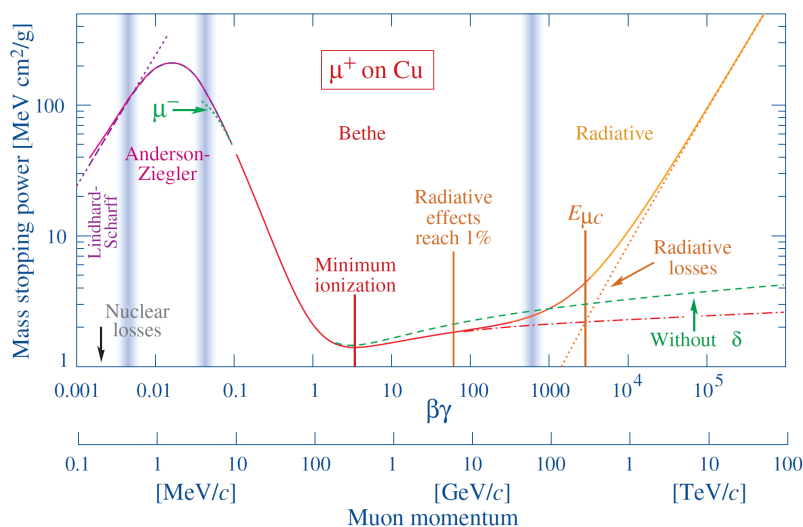


**Fig. 3:** Mass stopping power of positively charged muons in copper (solid line: total stopping power, dotted line: radiative stopping power, dash-dotted line: electronic stopping power according to Bethe). The figure originates from Ref. [4].

larger mass (e.g., hundreds of GeV for muons). High-energy muons can lose energy in Bremsstrahlung and electron–positron pair production processes, and they can also induce photonuclear interactions. The mean energy loss per unit length due to radiative losses is generally quantified by means of radiative stopping powers.

### 4.3 Energy loss of hadrons and muons

Figure 3 illustrates the mass stopping power of 100 keV/c–100 TeV/c muons in copper. Mass stopping power, which is generally expressed in  $\text{MeV}\cdot\text{cm}^2/\text{g}$ , is defined as the stopping power multiplied by the material density. The solid line shows the sum of electronic and radiative stopping powers. The latter are dominant above a few hundred GeV. Over a large energy range (above a few MeV), electronic stopping powers of muons and hadrons can be described by the well-known Bethe equation [25], with the addition of some higher-order corrections (density effect, Bloch and Barkas–Andersen correction terms, see Refs. [26–28]). To a first order, electronic mass stopping powers of hadrons and muons exhibit only a weak material dependency in the Bethe regime (with the exception of hydrogen), since they are proportional to  $Z/A$ . In addition, the stopping power depends on the velocity and charge of a projectile, but only very weakly on the projectile mass (via  $T_{\text{max}}$ ). The Bethe equation exhibits a distinct minimum around  $\beta\gamma \approx 3\text{--}3.5$ ; charged projectiles with such velocities are generally referred to as minimum ionizing particles. The mass stopping power of minimum ionizing particles is 1–2  $\text{MeV}\cdot\text{cm}^2/\text{g}$  in most materials. At lower energies, where the Bethe equation cannot be applied, electronic stopping powers are often described by empirical formulae (see, for example, ICRU Report 49 [29] for stopping powers of protons and alpha particles).

### 4.4 Energy loss of electrons or positrons and the radiation length, $X_0$

For electrons and positrons, which are much lighter than muons, radiative losses are already important at much lower energies. This is illustrated in Fig. 4, which shows electronic and radiative mass stopping powers of electrons in carbon and lead. Radiative losses start to dominate above a few tens of MeV in low- $Z$  materials, and above a few MeV in high- $Z$  materials. The energy, at which electronic and radiative

**Table 2:** Critical energy of electrons  $E_c$  and radiation length  $X_0$  for different materials. The values originate from Ref. [32]. The critical energy corresponds to Rossi's definition, which is slightly different from that given in Eq. (20). Rossi defines the critical energy as the energy where  $-dE/dx|_{\text{elec}} = E/X_0$ , see Ref. [4].

Material	$Z$	Density [g/cm <sup>3</sup> ]	$E_c$ [MeV]	$X_0$ [cm]
C	6	2.2	81.7	19.3
Al	13	2.7	42.7	8.90
Fe	26	7.8	21.7	1.76
Cu	29	8.96	19.4	1.44
W	74	19.3	8.0	0.35
Pb	82	11.4	7.4	0.56

stopping powers are equal is generally referred to as the critical energy  $E_c$  [4]:

$$\frac{dE_{\text{ion}}}{dx}(E_c) = \frac{dE_{\text{rad}}}{dx}(E_c). \quad (20)$$

Some numerical values of  $E_c$  for different materials are given in Table 2. As can be seen in Fig. 4, at higher energies, radiative stopping powers are linearly proportional to the electron energy, i.e., the mean energy loss can be written as

$$-\frac{dE}{dx} = \frac{E}{X_0}, \quad (21)$$

where the constant of proportionality,  $X_0^{-1}$ , is the inverse radiation length. It follows from this simple differential equation that the average energy of high-energy electrons decreases exponentially with travelled length:

$$\langle E(x) \rangle = E_0 \cdot \exp\left(-\frac{x}{X_0}\right), \quad (22)$$

where  $E_0$  is the energy at  $x = 0$ . The radiation length is therefore the average distance needed to reduce the energy of a high-energy electron by a factor of  $1/e$ . At the same time, the radiation length is also a characteristic length for the penetration of high-energy photons in matter. The pair production cross-section (see Fig. 2) and, therefore, the mean free path are constant at high energies and can be written as [4]

$$\sigma_{\text{pair}} \approx \frac{7}{9} \frac{M}{\rho N_A X_0}, \quad \lambda_{\text{pair}} \approx \frac{9}{7} X_0, \quad (23)$$

where  $M$  and  $\rho$  are the molar mass and the material density, respectively. This means that the radiation length is about  $7/9$  of the mean free path of high-energy photons and therefore determines the photon survival probability, i.e.,

$$I(x) = I_0 \cdot \exp\left(-\frac{7}{9} \frac{x}{X_0}\right), \quad (24)$$

where  $I(x)$  is the photon intensity at depth  $x$ . As will be discussed in Section 6.2, the radiation length is an important quantity for describing the longitudinal features of electromagnetic showers. The radiation length for different materials can be derived from the well-known formula from Tsai, as described in Ref. [4], but is commonly approximated by the following simplified expression [4]:

$$X'_0 = \frac{716.4 \text{ g/cm}^2 A}{Z(Z+1) \ln(287/\sqrt{Z})}, \quad (25)$$

where  $X'_0$  is  $X_0 \rho$  in g/cm<sup>2</sup>, and  $Z$  and  $A$  are the atomic and mass numbers, respectively. Some numerical values of the radiation length in different materials are given in Table 2.

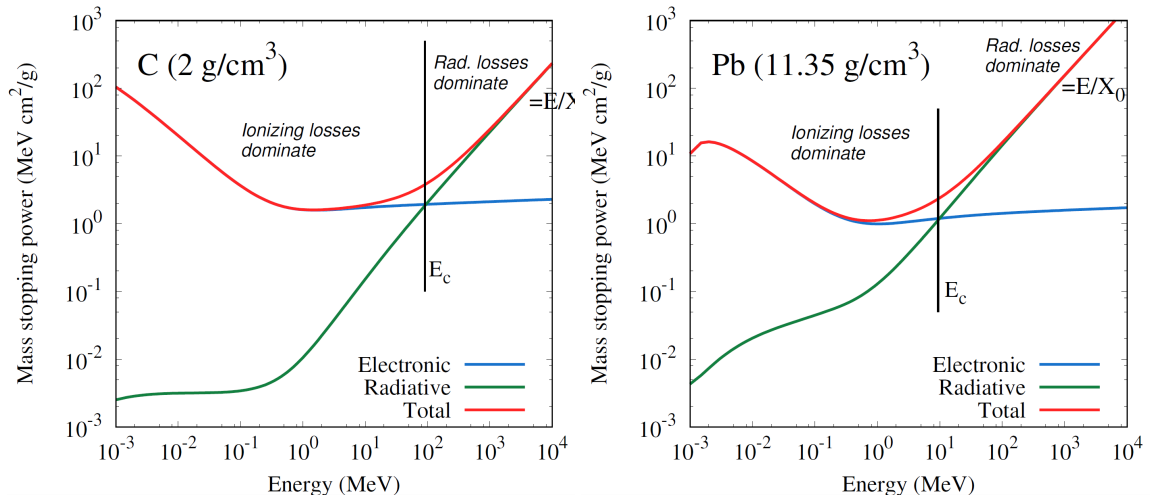


**Fig. 4:** Mass stopping powers of electrons in (left) carbon and (right) lead. The curves originate from the NIST ESTAR web database [30], which is based on tabulations from ICRU Report 37 [31]. The vertical lines indicate the critical energy defined in Eq. (20).

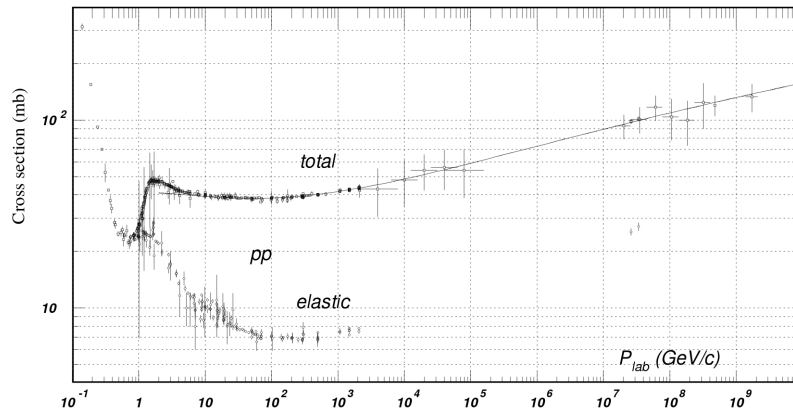


**Fig. 5:** Total and elastic proton–proton cross-sections. The figure originates from Ref. [4].

## 5 Nuclear interactions

### 5.1 Hadron–nucleus collisions

Hadrons travelling in matter can be subject to elastic and inelastic collisions with nuclei because of the strong force. Nuclear collisions are considered inelastic if new particles are produced or if the internal structure of the target nucleus or the projectile is changed. Some general features of nuclear collisions can be inferred from nucleon–nucleon cross-sections. Figure 5 shows total and elastic proton–proton cross-sections. The total cross-sections are the sum of the elastic and inelastic ones. As can be seen in the figure, above a few GeV, total cross-sections are relatively energy-independent up to the highest energies reached in today’s accelerators. Moreover, over a wide energy range, inelastic cross-sections are much larger than elastic ones.

The microscopic cross-section for inelastic hadron–nucleus cross-section scales approximately with  $A^{2/3}$ , which means that the mean free path  $\lambda$  shows the following material dependency:

$$\lambda \propto \frac{A^{1/3}}{\rho}. \quad (26)$$

**Table 3:** Inelastic scattering length of 7 TeV protons in different materials. The values derive from the FLUKA Monte Carlo code [18, 19].

Material	$Z$	Density [g/cm <sup>3</sup> ]	$\lambda$ [cm]
C	6	2.2	37.3
Al	13	2.7	35.4
Fe	26	7.8	15.1
Cu	29	8.96	13.9
W	74	19.3	8.9
Pb	82	11.4	15.7

The mean free path for inelastic collisions is generally known as the inelastic scattering length (as mentioned in Section 3.3). Table 3 lists the inelastic scattering lengths of 7 TeV protons in different elemental materials. The inelastic scattering length is a characteristic length for describing hadronic showers and is generally longer than the radiation length. Hadronic showers are therefore longer than electronic ones (see Section 6 for details).

Hadron–nucleus collisions have been described in more detail in the papers of Mokhov and Cerutti [3] and Ferrari [2]. A detailed account of nuclear reactions can also be found in Ref. [6]. The following description provides only a brief and very simplified picture of inelastic hadron–nucleus collisions at higher energies. In the initial fast stage of a hadron–nucleus interaction ( $10^{-22}$  s), the incident hadron interacts with the nucleons and new particles can be produced (in particular, pions) if the projectile energy is high enough (in particular for energies  $\geq$ GeV). If a nucleon collides with a free nucleon, pion production can occur at energies greater than 290 MeV [6]. The energy threshold is somewhat smaller for nucleons bound in a nucleus [6]. The hadrons (protons, neutrons, pions) can form intranuclear cascades and the more energetic particles can leave the nucleus. These fast particles are mainly forwards-directed and their multiplicity scales approximately with the logarithm of the incident particle energy. The other particles can deposit their energy in the nucleus and leave it in an excited state. After going through a pre-compound phase, the nucleus is subject to a slow de-excitation process ( $10^{-16}$  s). In this evaporation phase, lower-energy (MeV) neutrons, protons, or light fragments (alpha particles) are emitted isotropically. In addition, the residual nucleus can be subject to  $\gamma$  de-excitation. In heavy elements, evaporation competes with fission, where the nucleus breaks up in larger residuals. Fission products can also be subject to particle evaporation. The residual nuclei remaining from evaporation or fission can be radioactive.

## 5.2 Low-energy neutron interactions

Neutrons have a relatively long mean lifetime, of almost 15 min; hence, they are the only ‘stable’ neutral hadrons. Neutrons with energies of a few MeV will mainly slow down, owing to elastic scattering, until they are thermalized and captured by a nucleus. For illustration, Fig. 6 shows the cross-section of neutrons in <sup>56</sup>Fe as a function of the neutron energy (between  $10^{-4}$  eV and 20 MeV). The cross-sections have characteristic resonances because of the specific nuclear structure. Over a wide energy range, the elastic scattering cross-section dominates. Inelastic interactions, where one or more less-energetic neutrons are emitted from the target nucleus or the nucleus gets excited, occur above a threshold energy and contribute to the deceleration of neutrons in the MeV region. Other reaction channels exist as well, where protons, deuterons, or alpha particles are emitted. The cross-section for capture is inversely proportional to the neutron velocity and thermal neutrons are hence more likely to be absorbed than fast neutrons. Capture is often followed by gamma emission (radiative capture). In heavier materials, neutrons can also induce fission. Neutron absorption depends strongly on the nuclear isotopes contained in a material; different evaluated data libraries exist, in which neutron cross-sections are tabulated (e.g., ENDF/B-VII, JENDL); the tables can be accessed via a web-based interface [34].

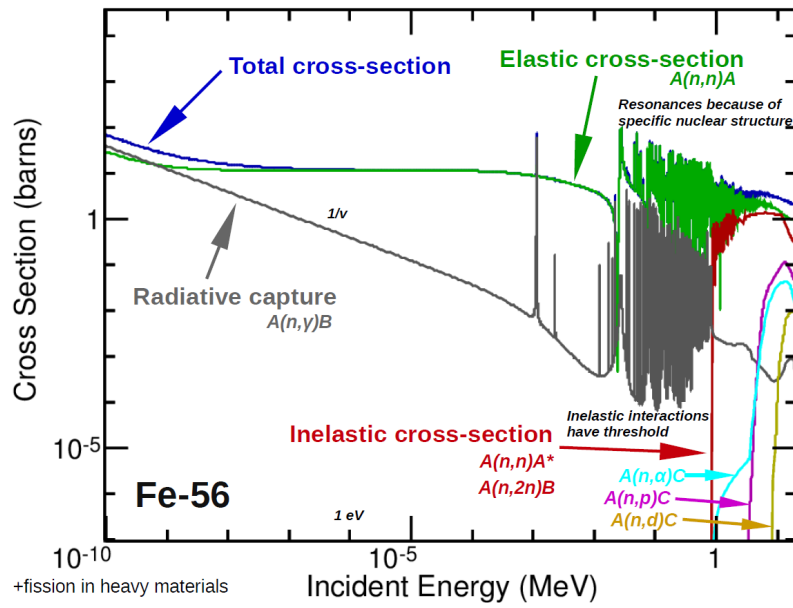


**Fig. 6:** Cross-sections of neutrons in  $^{56}\text{Fe}$ . The figure originates from the web-based interface of the ENDF/B-VII.1 database [33].

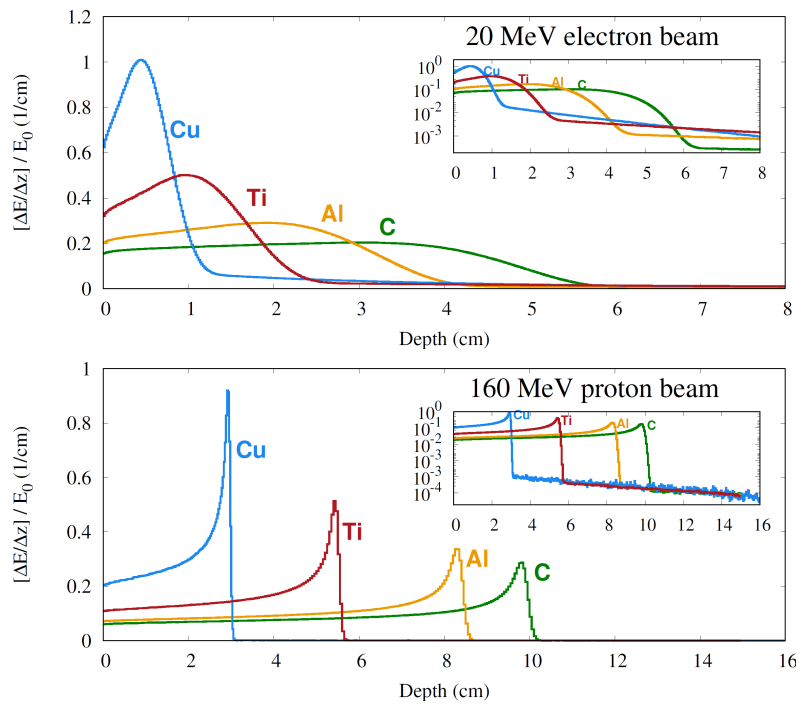


**Fig. 7:** Longitudinal energy deposition profiles of 20 MeV electron beams (top) and 160 MeV proton beams (bottom) in different materials. The profiles were obtained with the FLUKA Monte Carlo code and are expressed in the reduced form defined in Eq. (27). The inset figures are in logarithmic scale for a better visualization of the energy deposition tails.

## 6 Energy deposition and particle showers

The energy deposition in a material is mediated by Coulomb interactions of charged particles, which are set in motion by atomic and nuclear processes. The ionizing energy loss of a charged particle in a certain volume  $V$  can still be different from the energy deposition in  $V$ , since the energy can be transported away by  $\delta$ -rays. This section illustrates, by means of a few examples, the dependency of energy deposition profiles on particle type, energy, and target material. Section 6.1 addresses lower particle energies, where particle showers are irrelevant (MeV regime), while Sections 6.2 and 6.3 are dedicated to electromagnetic and hadronic showers, which determine the energy deposition at higher energies (GeV regime and above). To highlight characteristic features of energy deposition profiles, it is assumed that a pencil beam impacts a laterally infinite material block. The longitudinal energy deposition profiles shown throughout this section are expressed as

$$\varepsilon(z_i) = \frac{1}{E_0} \frac{\Delta E(z_i)}{\Delta z}, \quad (27)$$

where  $E_0$  is the incident particle energy and  $\Delta E(z_i)$  is the energy deposited in the layer between  $z_i$  and  $z_i + \Delta z$ . In this form, energy deposition profiles are more easily comparable, since the area under the curves is identical (except for cases involving nuclear interactions, where a fraction of energy is needed to overcome the binding energy). Depending on the particle type and energy, the longitudinal co-ordinate is substituted by a characteristic length, such as the radiation length (electromagnetic showers) or the inelastic scattering length (hadronic showers).

### 6.1 Energy deposition by lower-energy particles (MeV regime)

Figure 7 illustrates energy deposition profiles of 20 MeV electron beams in different materials. The profiles are characterized by an initial build-up region, which is followed by a broad peak. The shape of the peak is much governed by the Coulomb scattering of electrons as they slow down. The profiles have a long tail induced by Bremsstrahlung photons, which can travel much further than the electrons. The tail is more pronounced in heavier materials, since the critical energy is lower and radiative losses are hence more important ( $E_c$  is roughly 80 MeV for carbon and about 20 MeV for copper, see Table 2).

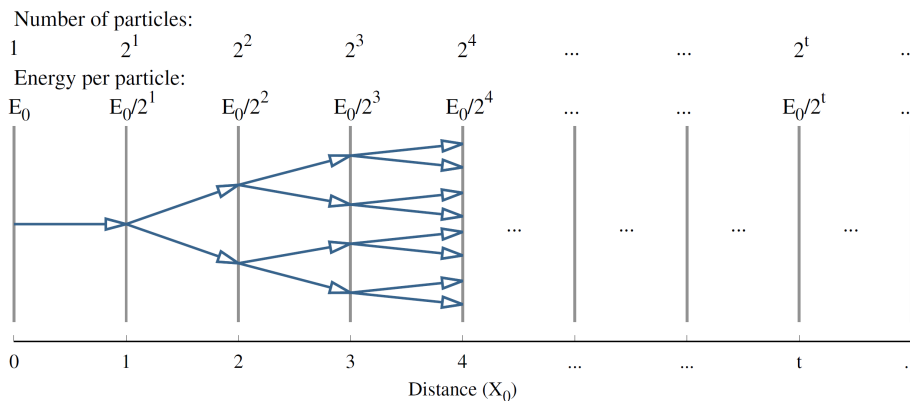


**Fig. 8:** Multiplication of electromagnetic cascade particles in the toy model of Heitler. The incident particle can be either an electron or positron or a photon. The longitudinal co-ordinate is expressed in terms of radiation lengths.

The energy deposition profiles of MeV protons (up to some hundreds of MeV) are characterized by a distinct peak, which is referred to as the Bragg peak. Compared with electrons, the angular deflection of protons as they slow down is much smaller and many protons stop within a certain depth range. Since the average energy loss per unit length is higher towards the end of their range (see Bethe formula), the energy deposition rises sharply before the protons stop. The exact shape of the Bragg peak

is determined by the beam energy spread, the energy loss straggling, and Coulomb and nuclear elastic scattering processes, but also by inelastic nuclear interactions, which become increasingly important at higher energies. Figure 7 illustrates the Bragg peak of 160 MeV protons in different materials. Beyond the peak, the energy deposition profiles feature a long tail, which is due to neutrons. Ions exhibit a similar Bragg peak as protons, but the tail beyond the peak is more pronounced because of secondary particles produced in the fragmentation of ions.

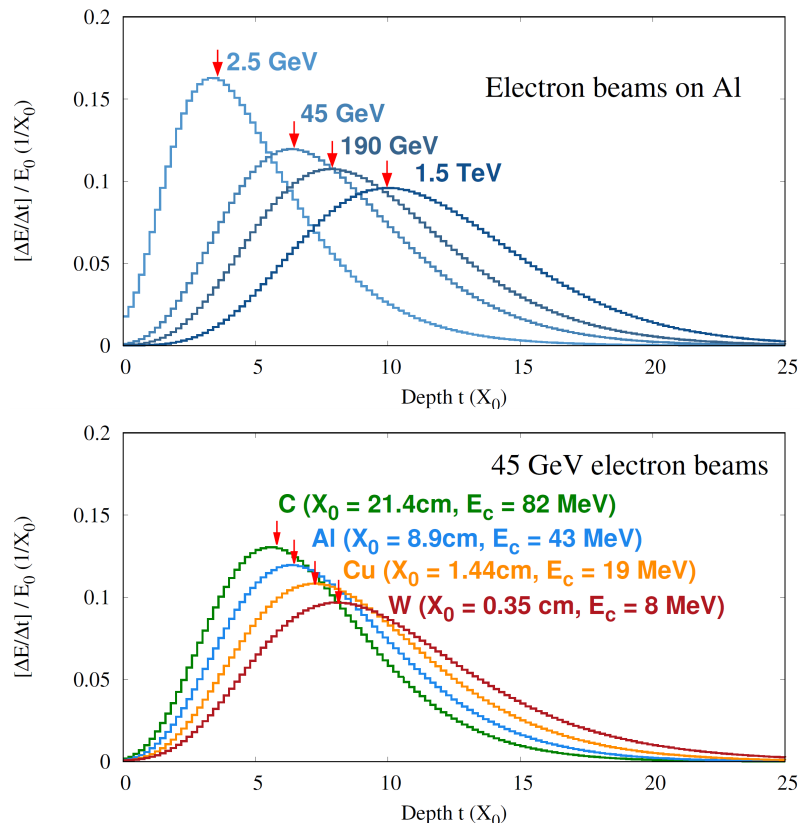


**Fig. 9:** Longitudinal energy deposition profiles of (top) 2.5 GeV–1.5 TeV electron beams in aluminium and (bottom) 45 GeV electron beams in carbon, aluminium, copper, and tungsten. The beam energies correspond to the operational energies of past and future machines: KEK/PF linac (2.5 GeV), LEP at start-up (45 GeV), CLIC stage 1 (190 GeV), and CLIC stage 3 (1.5 TeV). The profiles were obtained with the FLUKA Monte Carlo code and are expressed in the reduced form defined in Eq. (27). The longitudinal co-ordinate is given in terms of radiation lengths. The red arrows indicate the position of the shower maximum, as predicted by Eq. (31).

## 6.2 Electromagnetic showers

As discussed in Section 4, high-energy electrons and positrons mainly lose energy through Bremsstrahlung processes, whereas high-energy photon interactions are dominated by electron–positron pair production. If the energy of an incident electron, positron or photon is high enough ( $\geq \text{GeV}$ ), these processes give rise to a particle multiplication, which is referred to as an electromagnetic shower. The average particle energy decreases from shower generation to shower generation and the cascade development approximately ceases when the energy of electrons and positrons falls below the critical energy,  $E_c$ , where ionization and excitation processes become dominant.

The location where the number of cascade particles is a maximum is referred to as the shower maximum. Since the radiation length  $X_0$  is a characteristic length for Bremsstrahlung and pair production

processes, it is also a central quantity for describing the longitudinal development of electromagnetic showers. Some qualitative features of the longitudinal shower profile can be derived from Heitler's model [35], which assumes that interactions (Bremsstrahlung and pair production) always take place after a distance  $X_0$  and that, at each interaction, the energy is equally split between the two outgoing particles. In this simple model, the number of particles after  $t$  radiation lengths is given by

$$N(t) = 2^t \quad (28)$$

and the energy per particle is

$$E(t) = E_0/2^t, \quad (29)$$

where  $E_0$  is the energy of the incident particle (see Fig. 8). If one assumes that the cascade stops, i.e., reaches its maximum, when the energy per particle is equal to  $E_c$ , then it follows from Eq. (29) that the depth of the maximum,  $t_{\max}$ , depends logarithmically on the initial energy:

$$t_{\max} \propto \log \left( \frac{E_0}{E_c} \right). \quad (30)$$

Since  $t_{\max}$  expresses the depth of the shower maximum in terms of radiation lengths, and since  $X_0$  is approximately proportional to  $A/Z^2\rho$  (see Section 4), it follows that electromagnetic showers are shorter the higher the atomic number and the higher the material density. If one inserts Eq. (30) into Eq. (28), one can also see that the shower size, i.e., the number of particles at the maximum, increases with the initial particle energy.

Although the Heitler model provides a qualitative description of the longitudinal shower development, it fails to predict absolute particle numbers or relative features, such as the ratio of electrons or positrons and photons at the shower maximum. In reality, there is an excess of photons, since Bremsstrahlung photons are much more frequently produced than is assumed in the Heitler model. In addition, the model neglects other processes, such as Compton scattering and the photoelectric effect, which lead to the production of low-energy electrons. These electrons are important for dissipating the energy carried by the shower.

A more accurate description of the electromagnetic shower development can be obtained from Monte Carlo simulations. Figure 9 shows longitudinal energy deposition profiles of electron beams in different materials. The profiles were obtained using the FLUKA shower simulation code [18, 19]. The longitudinal co-ordinate is expressed in terms of radiation length. The two plots demonstrate the dependency on the beam energy  $E_0$  and the target material ( $E_c$ ), respectively. In higher- $Z$  materials, where the critical energy  $E_c$  is lower, the multiplication process continues down to lower energies and the shower maximum therefore occurs at larger depths (in terms of  $X_0$ ). The red arrows in the plots indicate the position of the shower maximum predicted by the following empirical formula [4]:

$$t_{\max} = \log \left( \frac{E_0}{E_c} \right) - 0.5. \quad (31)$$

The formula applies to electron- and positron-induced showers, while the latter term has to be replaced by '+0.5' for photon-induced showers [4]. This small difference results from the different nature of the initial interactions and is, by construction, not predicted by the Heitler model. Beyond the shower maximum, the energy deposition profiles do not scale with  $X_0$ , since other processes than Bremsstrahlung and pair production become dominant. The longitudinal shower tails decay more rapidly in lower- $Z$  materials.

The transverse profile of the shower core around the shower maximum is roughly independent of the beam energy. The lateral shower opening is mainly governed by the multiple scattering of lower-energy electrons. Lateral features of the shower core can be well described by the Molière radius  $R_M$ ,

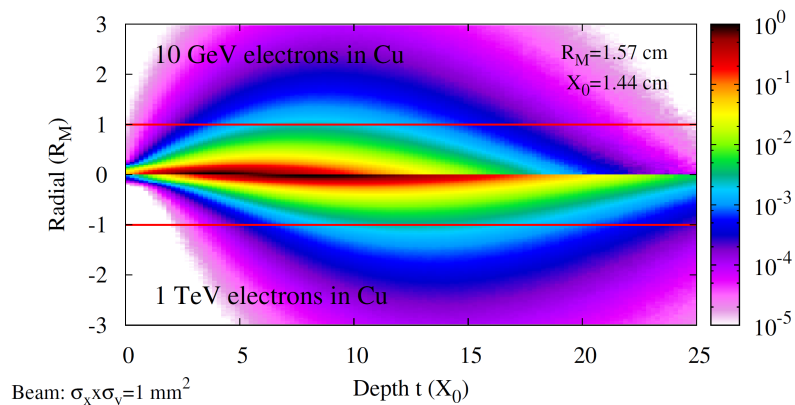


**Fig. 10:** Two-dimensional energy density maps for (top half) 10 GeV and (bottom half) 1 TeV electron beams incident on copper. The profiles were obtained with FLUKA Monte Carlo simulations and are normalized to the maximum energy density. The longitudinal co-ordinate is given in terms of radiation lengths and the radial co-ordinate in terms of Molière radii. The assumed beam size ( $\sigma$ ) is 1 mm.

which represents the average lateral deflection of electrons with  $E = E_c$  after traversing one radiation length  $X_0$  [4]:

$$R_M = \frac{\sqrt{4\pi\alpha m_e c^2}}{E_c} X_0 \approx \frac{21 \text{ MeV}}{E_c} X_0, \quad (32)$$

where  $\alpha$  is the fine structure constant, and  $m_e c^2$  is the electron mass. Typically, a large fraction of the beam energy (>90%) is deposited within a cylinder with a radius of  $R_M$  around the beam axis (if the beam size is much smaller than  $R_M$ ). For illustration, Fig. 10 shows two-dimensional energy density maps for 10 GeV and 1 TeV electron beams incident on copper. The radial energy density profile at the shower maximum is comparable for the two energies.

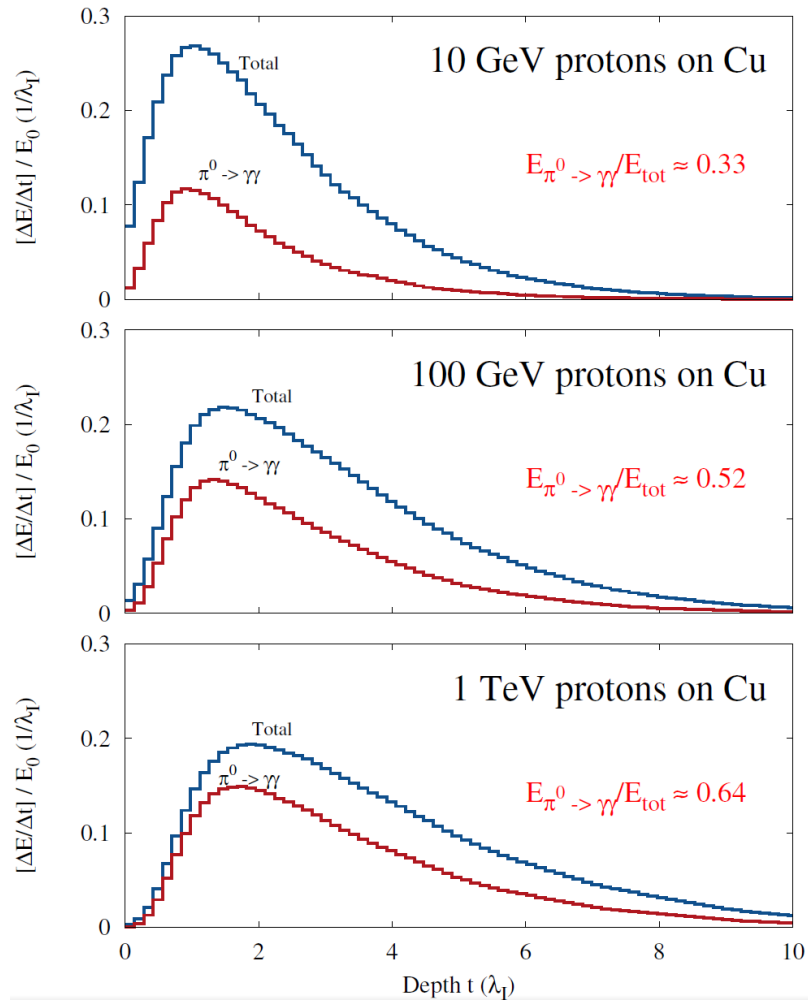


**Fig. 11:** Longitudinal energy deposition profiles of (top) 10 GeV, (centre) 100 GeV, and (bottom) 1 TeV proton beams in copper. Profiles were calculated with the FLUKA Monte Carlo code and are expressed in the reduced form defined in Eq. (27). Blue curves indicate the total energy deposition, while red curves show the energy deposited by electromagnetic showers initiated by  $\pi^0 \rightarrow \gamma\gamma$ .

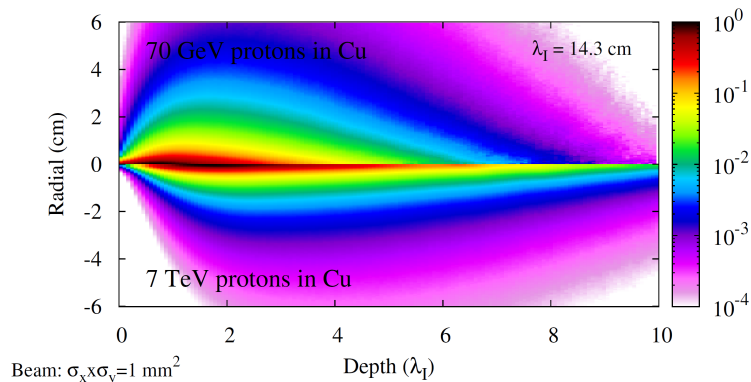


**Fig. 12:** Two-dimensional energy density maps for 70 GeV (top half) and 7 TeV (bottom half) proton beams incident on copper. The profiles were obtained with FLUKA Monte Carlo simulations and are normalized to the maximum energy density. The longitudinal co-ordinate is given in terms of inelastic scattering lengths. The assumed beam size ( $\sigma$ ) is 1 mm.

### 6.3 Hadronic showers

If a high-energy hadron undergoes an inelastic nuclear collision in a material, the energetic, mainly forwards-directed collision products (n, p,  $\pi^{+/-}$ , ...) will be subject to further collisions. Since, on average, several hadrons are produced in each collision, the re-interaction of secondary products gives rise to a particle multiplication, which is called a hadronic shower. Since the multiplication process is governed by inelastic collisions, the longitudinal shower development can be characterized by the inelastic scattering length  $\lambda$ , introduced in Section 5. A non-negligible fraction of the initial energy can go into binding energy or can be transferred to recoils. Lower-energy particles are produced in evaporation, gamma de-excitation, and fission, and some energy is also carried away by neutrinos. The multiplication process roughly continues until the energy falls below the pion production threshold. As for electromagnetic showers, the shower length, i.e., the depth of the shower maximum, increases logarithmically with energy.

Hadronic showers also have an electromagnetic component, owing to the production of neutral pions, which decay into energetic  $\gamma$  pairs (neutral pions also have other decay channels, but with smaller branching ratios). Other secondary particles can also induce electromagnetic showers (e.g.,  $\eta$  mesons), but they are produced with much smaller multiplicities. The electromagnetic shower component is mainly concentrated around the shower core, since electromagnetic showers are narrower than hadronic ones. In addition, they are shorter since the radiation length is generally much smaller than the inelastic scattering length (compare Tables 2 and 3). While hadronic showers can transfer a significant fraction of energy to electromagnetic showers, the coupling in the other direction is much weaker. Hadrons can be produced in photonuclear or electronuclear interactions, but the cross-sections of these processes are small and the fraction of energy transferred back to hadrons is often negligible. Photonuclear or electronuclear processes can still be of importance for some applications (e.g., neutron production in electron accelerators).

The fraction of energy dissipated by the electromagnetic shower component increases with particle energy. At each nuclear interaction, about one-third of the energy is carried away by  $\pi^0$ s. Conversely, the higher the initial energy, the more interactions are needed, such that hadrons in the cascade reach GeV energies and the shower eventually ceases. As a consequence, the contribution of electromagnetic showers to the energy deposition increases and becomes dominant at higher energies. This is illustrated in Fig. 11, which shows longitudinal energy deposition profiles of 10 GeV, 100 GeV, and 1 TeV proton beams in copper. The longitudinal co-ordinate is expressed in terms of inelastic scattering lengths. At 100 GeV, about one-half of the initial energy is dissipated by  $\gamma$ -induced showers.

The transverse momentum of hadrons produced in nuclear collisions is more or less invariant with energy (the average being 300–400 MeV/c) [6]. As a consequence, the shower opening angle becomes narrower with increasing energy. This in turn also leads to a greater overlap of electromagnetic showers around the core. Figure 12 shows two-dimensional energy density maps for 70 GeV and 7 TeV beams incident on copper. The radial profile drops more sharply in the latter case.

## Acknowledgements

The author thanks F. Cerutti for proofreading the manuscript.

## References

- [1] A. Ferrari, A primer on particle interactions with matter, (CERN, Geneva, 2011).
- [2] A. Ferrari, Interactions of particles with matter, CERN Accelerator School, Accelerators for Medical Applications, Vösendorf, 2015.
- [3] N.V. Mokhov and F. Cerutti, Beam–material interactions, Proc. 2014 Joint International Accelerator School: Beam Loss and Accelerator Protection, Newport Beach, CA, USA, 5-14 November 2014, CERN-2016-002 (CERN, Geneva, 2016) p. 83. <http://dx.doi.org/10.5170/CERN-2016-002>.
- [4] C. Patrignani *et al.* (Particle Data Group), *Chin. Phys. C* **40** (2016) 100001, updated 2017, <https://doi.org/10.1088/1674-1137/40/10/100001>.
- [5] P. Sigmund, *Particle Penetration and Radiation Effects*, (Springer-Verlag, Berlin, 2006).
- [6] A. Ferrari and P.R. Sala, Proc. Workshop on Nuclear Reaction Data and Nuclear Reactors, Physics, design and safety, Trieste, Italy, 15 April-17 May 1996, Eds. A. Gandini and G. Reffo (World Scientific, Singapore, 1998), p. 424, <https://doi.org/10.1142/9789814530385>.
- [7] B.B. Rossi, *High-Energy Particles*, (Prentice-Hall, New York, 1952).
- [8] LHC Design Report, edited by O.S. Brüning, P. Collier, P. Lebrun, S. Myers, R. Ostojic, J. Poole and P. Proudlock, CERN-2004-003-V-1, (CERN, Geneva, 2004), <http://dx.doi.org/10.5170/CERN-2004-003-V-1>.
- [9] N.V. Mokhov *et al.*, Protecting LHC IP1/IP5 components against radiation resulting from colliding beam interactions, LHC-Project-Report-633, 2003.
- [10] R. Bruce *et al.*, *Phys. Rev. ST Accel. Beams* **12** (2009) 071002, <https://doi.org/10.1103/PhysRevSTAB.12.071002>.
- [11] R. Bruce *et al.*, *Nucl. Instr. Meth. Phys. Res. A* **729** (2013) 825, <https://doi.org/10.1016/j.nima.2013.08.058>.
- [12] F. Zimmermann *et al.*, Trapped macroparticles in electron storage rings, Proc. 1995 Particle Accelerator Conf., Dallas, TX, USA, 1995 (IEEE, Piscataway, 1996), p. 517, <https://doi.org/10.1109/PAC.1995.504705>.
- [13] T. Baer *et al.*, UFOs in the LHC, Proc. 2nd International Particle Accelerator Conf., TUPC137, San Sebastian, Spain, 2011, Ed. C. Petit-Jean-Genaz (EPS-AG, Geneva, 2011), p. 1347, <http://accelconf.web.cern.ch/AccelConf/IPAC2011/index.htm>.
- [14] G. Papotti *et al.*, Macroparticle-induced losses during 6.5 TeV LHC operation, Proc. 7th International Particle Accelerator Conf., TUPMW023, Busan, Korea, 2016, Eds. K.S. Kim, C. Petit-Jean-Genaz, I.S. Ko, K.R. Kim and V.R.W. Schaa (JACoW, Geneva, 2016), p. 1481, <http://dx.doi.org/10.18429/JACoW-IPAC2016-TUPMW023>.
- [15] H. Vincke *et al.*, *Radiat. Prot. Dosimetry* **146** (2011) 434, <https://doi.org/10.1093/rpd/ncr245>.
- [16] B. Auchmann *et al.*, *Phys. Rev. ST Accel. Beams* **18** (2015) 061002, <https://doi.org/10.1103/PhysRevSTAB.18.061002>.

- [17] M. Brugger, Radiation damage to electronics at the LHC, Proc. 3rd International Particle Accelerator Conf., MOPPC004, New Orleans, LA, USA, 2012, Eds. F. Zimmermann and C. Eyberger (IEEE, Piscataway, 2012), p. 3734.
- [18] T.T. Böhlen *et al.*, *Nucl. Data Sheets* **120** (2014) 211, <https://doi.org/10.1016/j.nds.2014.07.049>.
- [19] A. Ferrari *et al.*, FLUKA: a multi-particle transport code, CERN-2005-10, INFN/TC\_05/11, SLAC-R-773 (CERN, Geneva, 2005), <http://dx.doi.org/10.5170/CERN-2005-010>.
- [20] L. Landau, *J. Phys. USSR* **8** (1944) 201.
- [21] P.V. Vavilov, *Sov. Phys. JETP* **5** (1957) 749.
- [22] P.V. Vavilov, *Zh. Eksp. Teor. Fiz.* **32** (1957) 920.
- [23] G. Molière, *Z. Naturforsch. A* **3** (1948) 78.
- [24] H.A. Bethe, *Phys. Rev.* **89** (1953) 1256, <https://doi.org/10.1103/PhysRev.89.1256>.
- [25] H.A. Bethe, *Ann. Phys.* **397** (1930) 325, <https://doi.org/10.1002/andp.19303970303>.
- [26] F. Bloch, *Ann. Phys.* **408** (1933) 285, <https://doi.org/10.1002/andp.19334080303>.
- [27] S. P. Ahlen, *Phys. Rev. A* **17** (1978) 1236, <https://doi.org/10.1103/PhysRevA.17.1236>.
- [28] J. C. Ashley *et al.*, *Phys. Rev. B* **5** (1972) 2393, <https://doi.org/10.1103/PhysRevB.5.2393>.
- [29] M. J. Berger *et al.*, *J. Int. Commission Radiat. Units Measurements* **25** (1993), <https://doi.org/10.1093/jicru/os25.2.Report49>.
- [30] <https://physics.nist.gov/PhysRefData/Star/Text/ESTAR.html>, last accessed January 30th, 2018.
- [31] M. J. Berger *et al.*, *J. Int. Commission Radiat. Units Measurements* **19** (1984), <https://doi.org/10.1093/jicru/os19.2.Report37>.
- [32] <http://pdg.lbl.gov/2017/AtomicNuclearProperties/>, last accessed January 30th, 2018.
- [33] <http://www.nndc.bnl.gov/exfor/endl00.jsp>, last accessed January 30th, 2018.
- [34] <https://www-nds.iaea.org/exfor/endl.htm>, last accessed January 30th, 2018.
- [35] W. Heitler, *The Quantum Theory of Radiation*, (Clarendon Press, Oxford, 1954).